ACS OMEGA

Open Access

http://pubs.acs.org/journal/acsodf

Article

Research on CCHP Design and Optimal Scheduling Based on Concentrating Solar Power, Compressed Air Energy Storage, and Absorption Refrigeration

Xinglin Yang,* Shouqing Zheng, and Jiaqi Chang

Cite This: *ACS Omega* 2023, 8, 42126−42143

Read Online

ACCESS | Metrics & More | Article Recommendations

ABSTRACT: In response to the country's "carbon neutrality, peak carbon dioxide emissions" task, this paper constructs an integrated energy system based on clean energy. The system consists of three subsystems: concentrating solar power (CSP), compressed air energy storage (CAES), and absorption refrigeration (AR). Among them, thermal energy storage equipment in the photothermal power generation system can alleviate the fluctuation of solar energy and provide a stable power supply for the system. The compression heat generated during the compression process of the CAES system can be recovered through heat transfer oil to provide a heat load. The compressed air in the air accumulator (ACC) expands in the air turbine to provide an electric load. The low-temperature exhaust gas discharged from the turbine can provide cool load. First, a multienergy system that includes CSP, CAES, and AR is built. Then, the system takes the lowest economic cost as the objective function and constructs the system day-ahead scheduling model. Finally, for data obtained from scene reduction, the commercial optimization software Gurobi is invoked through YALMIP to solve the model. The results show that the three subsystems achieve multienergy complementarity; system operating costs are reduced by 59.94% and fully absorb wind and solar energies by the system.

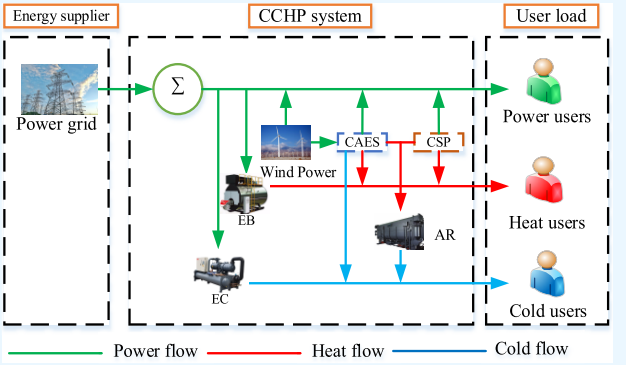

1. INTRODUCTION

The increasing prominence of energy and environmental issues has accelerated the development of new energy generation technology, and increasing the penetration rate of renewable energy and achieving a clean energy supply have received widespread attention both domestically and internationally. Among them, solar and wind energy, as the main renewable energy sources, have an increasing proportion of installed capacity year by year; however, renewable energy has intermittency and volatility, which can easily lead to the abandonment of wind and solar energies.[1]

To solve the above problems, energy storage technology can be used for peak load shifting, thereby reducing fluctuations caused by renewable energy and improving system stability. The energy storage technology applied in this article includes thermal energy storage and compressed air energy storage.[2]

Research on solar power generation technology can be divided into two categories: one is the use of solar cells to directly convert solar energy into electricity, that is, photovoltaic power generation; another category is to convert concentrated sunlight into thermal energy through heat transfer media and then convert it into electrical energy, namely, concentrated solar power (CSP) or photothermal power generation. This technology has higher power generation efficiency compared to photovoltaic power generation technology, so this study belongs to this category.[3] In the CSP system, thermal energy storage technology can be considered to suppress fluctuations in sunlight.[4] Thermal energy storage technology can store solar energy during low load periods and release it during peak load periods. Reference 5 points out that solar tower technology has superior power generation efficiency and expansion potential, among which the S-CO_2 Brayton cycle has superior thermodynamic performance and compact layout, making it a good power generation cycle system for photothermal power plants. In the study of coupling between photothermal power plants and subsystems such as the S-CO_2 Brayton cycle, ref 6 established a comprehensive solar power tower (SPT) system model based on the S-CO_2 recompression Brayton cycle, using the genetic algorithm for parameter optimization to achieve maximum total

Received: May 16, 2023
Revised: October 8, 2023
Accepted: October 9, 2023
Published: November 2, 2023

exergy efficiency. Reference 7 constructed various different layouts of S-CO_2 Brayton cycle systems integrated with SPT. Through comparative analysis, it was found that the recompression cycle layout has higher efficiency than the precompression cycle layout while the precompression cycle layout has higher stability in practical applications. The intercooling cycle layout and partial-cooling cycle layout have the best performance. Reference 17 proposes a novel SPT system combined with a cascaded S-CO_2 Brayton steam Rankine cycle, which has the advantages of high efficiency, large storage capacity, and short investment payback period. Therefore, in this work, the cascaded S-CO_2 Brayton steam Rankine cycle is used in photothermal power generation.

Research on wind power generation technology mainly focuses on the issue of wind power consumption, which is often solved through energy storage technology.[8] Currently, electric energy storage technologies mainly include pumped storage, battery energy storage, compressed air energy storage, and flywheel energy storage. Among them, CAES technology is considered a promising technology with the advantages of reliable operation, low construction cost, and environmental friendliness, and has received widespread attention from domestic and foreign scholars.[9] Internationally, Germany has planned to build the world's first large-scale advanced adiabatic compressed air energy storage (AA-CAES) power station, with a rated power of 90 MW, a rated capacity of 360 MW·h, and a target cycle efficiency of 70%.[10] In May 2017, NRStor and HydroStor companies in Canada promoted the joint development of large-scale CAES technology and are currently constructing an CAES experimental power plant with a salt cavern gas storage capacity of 1.75 MW/7 MW·h in Goderich, Canada.[11] In order to improve the economic benefits of CAES, ref 12 studied the capacity configuration of compressed air energy storage systems under wind energy uncertainty conditions. At the same time, an optimization model was established to maximize the investment return and minimize the volume of gas storage tanks, providing new ideas for the rationalization of power dispatch. Reference 13 established a reserve capacity model for CAES and participated in the operation of the power system, reducing the operating cost of the system while consuming wind power. The above research focuses less on the storage and utilization of waste heat in compressed air energy storage systems. This article considers the introduction of a small capacity absorption refrigeration device for secondary utilization of waste heat.

In order to integrate the above technologies into a system and leverage the excellent performance of each component, the problem can be solved through CCHP technology. At present, relevant research has been conducted. Reference 14 proposed a CCHP system that combines solar energy and CAES to improve the stability and energy utilization of the system's power supply. The research shows that the performance of a cogeneration system is mainly determined by the compressor pressure ratio, turbine inlet pressure and temperature, and efficiency of the heat exchanger. Scholars have also proposed a mathematical model for CCHP systems based on CAES systems, exploring the relationship between CAES system types, compression/expansion stages, and system parameters.[15] They have also adopted multiobjective optimization methods that consider three objective functions to optimize the design of different systems. Reference 16 proposed a CAES offshore multi energy complementary system based on wave energy, wind energy, and solar energy to promote the consumption of new energy, achieving efficient utilization of energy in coastal areas. Although the above literature considers photothermal energy as the external heat source of CAES, it does not consider integrating CSP technology and the S-CO_2 Brayton cycle into the CAES system.

Taking into account the above research, this article constructs a multi energy system model that includes CSP, CAES, and AR based on the cascaded S-CO_2 Brayton steam Rankine cycle. The main work content and innovation are as follows:

a Considering the three subsystems of CSP, CAES, and AR, a CCHP system is constructed to provide users with cooling, heating, and electrical loads.
b The photothermal power generation system is used to convert solar energy into electrical energy, alleviate solar energy fluctuations through molten salt heat storage equipment, and reduce system operating costs by using solar tower technology and the cascaded S-CO_2 Brayton steam Rankine cycle.
c The compressed air energy storage system is used to absorb wind power and achieve "peak load shifting". The absorption refrigeration cycle is embedded in the compressed air energy storage system, providing cooling load for the system by recovering the system's waste heat.
d The waste heat from CSP and the compression heat generated by CAES can be recycled through thermal oil circulation, which can not only provide heating load for users but also provide heat for absorption refrigeration.
e Taking the power purchase cost as the objective function, and considering the cooling and heating load demand of users and the time-of-use price, the day-ahead scheduling model of the CCHP system is established. Finally, in MATLAB, the Gulobi solver is called through YALMIP to analyze the model and perform operational and economic analysis on the system.

2. SYSTEM DESCRIPTION

The CCHP system based on CSP, CAES, and AR proposed in this paper consists of a conventional CCHP system and a power station, as shown in Figure 1. Conventional CCHP systems do not consider the utilization of wind energy, solar energy, and other renewable resources; they only consider the time-of-use electricity price of the power grid. Electric energy is directly purchased from a large power grid. The heat load is provided by an electricity boiler (EB), and the cooling load is provided by an electricity chiller (EC). The power station in Figure 1 includes three subsystems: CSP, CAES, and AR. This section will discuss

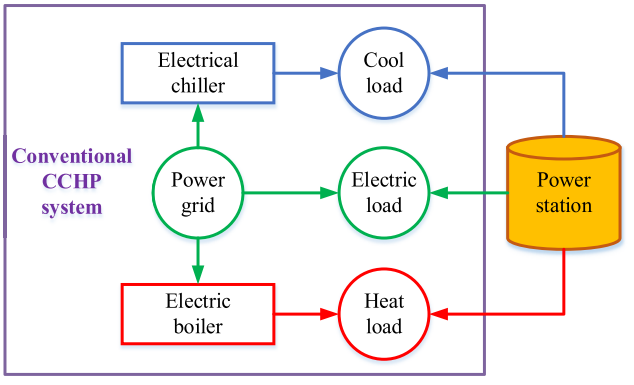

Figure 1. CCHP system based on CSP, CAES, and AR.

https://doi.org/10.1021/acsomega.3c03401
ACS Omega 2023, 8, 42126−42143

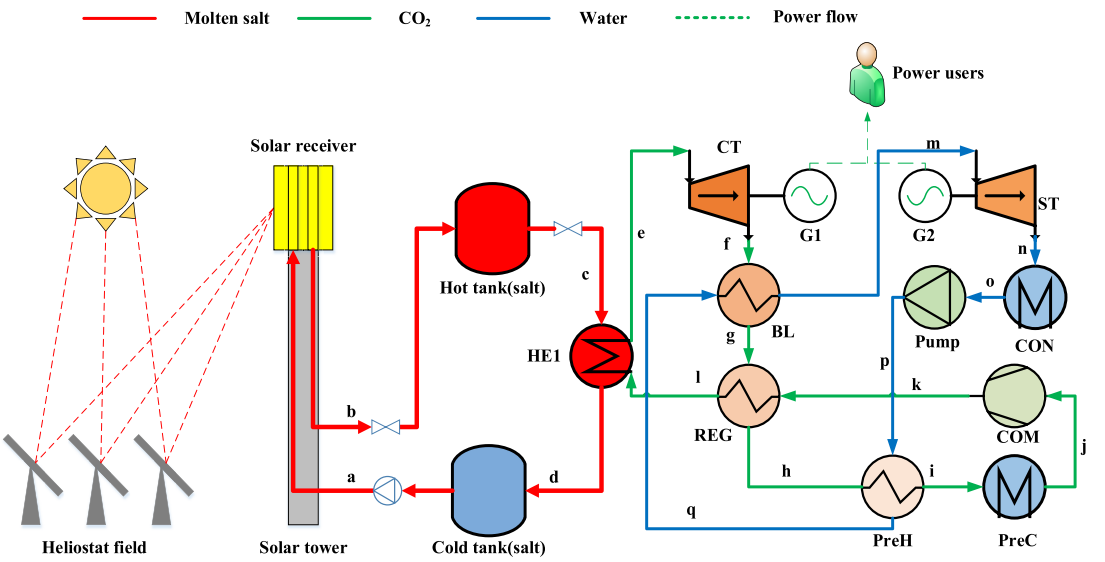

Figure 2. Power station 1 system schematic.

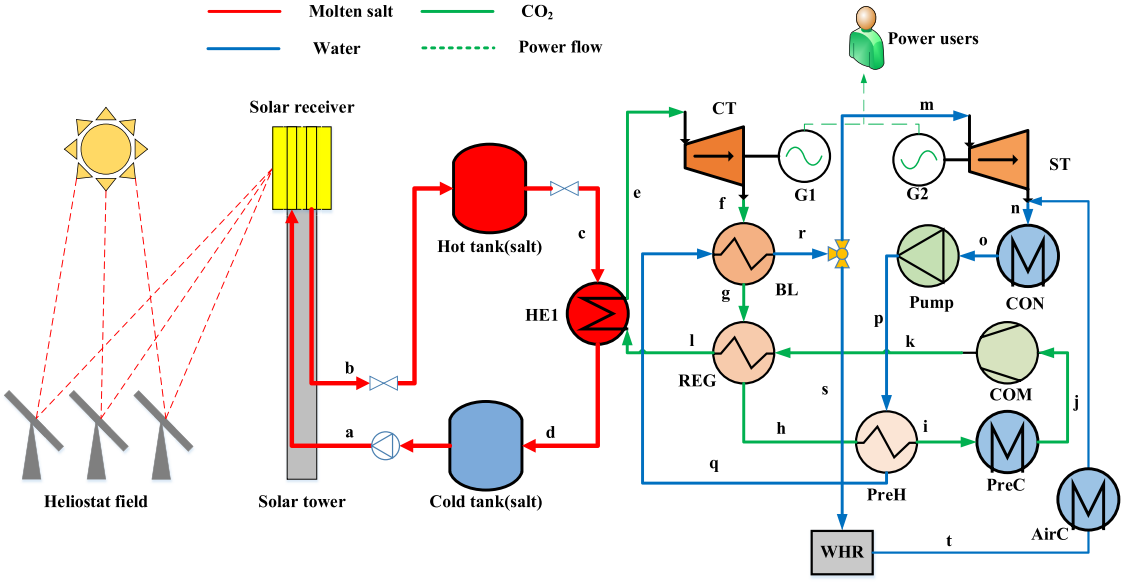

Figure 3. Power station 2 system schematic.

the establishment process and working principle of the system in detail.

2.1. Power Station 1. Conventional CCHP systems do not consider the use of renewable energy, and Power Station 1 introduces CSP to utilize solar energy. Considering the performance advantages of cascaded cycles, Power Station 1 adopts an efficient and compact SPT system with a cascaded S-CO_2 Brayton-steam Rankine cycle.[17] The system schematic diagram is shown in Figure 2. The system consists of a solar power tower, two molten salt heat storage tanks, and a cascaded S-CO_2 Brayton-steam Rankine cycle.

The molten salt cycles (a−d) in the system work as follows: When the SPT works, the heliostat field reflects sunlight on the receiver. The molten salt in the low-temperature molten salt heat storage tank is pumped to the receiver and heated to 565 °C. The heated molten salt flows into the high-temperature molten salt heat storage tank. When CO_2 flows into the cold side of HE1, the molten salt in the high-temperature molten salt heat storage tank flows into heat exchanger 1 (HE1), exchanges heat to CO_2, and finally returns to the low-temperature molten salt heat storage tank.

The process of the power generation cycle (e−q) is as follows:

a S-CO_2 Brayton cycle: CO_2 at low temperature and low pressure (32 °C, 7.5 MPa) enters the compressor (COM) to pressurize to 25 MPa. Then, it flows through REG for heat exchange and temperature rise and enters HE1 for heating to 550 °C. CO_2 enters the CO_2 turbine (CT) to expand and work and then flows into the boiler (BL) to heat the steam, and CO_2 from the BL enters the pre-heater (PreH) to preheat the steam and then flows into the precooler for cooling to complete the cycle.

b Steam Rankine cycle: The water pump pumps water into PreH for preheating, and the heated steam enters BL to be heated again to become high-temperature steam and then enters the steam turbine to do work, and the exhaust gas flows into the condenser to cool down, completing the cycle.

https://doi.org/10.1021/acsomega.3c03401
ACS Omega 2023, 8, 42126−42143

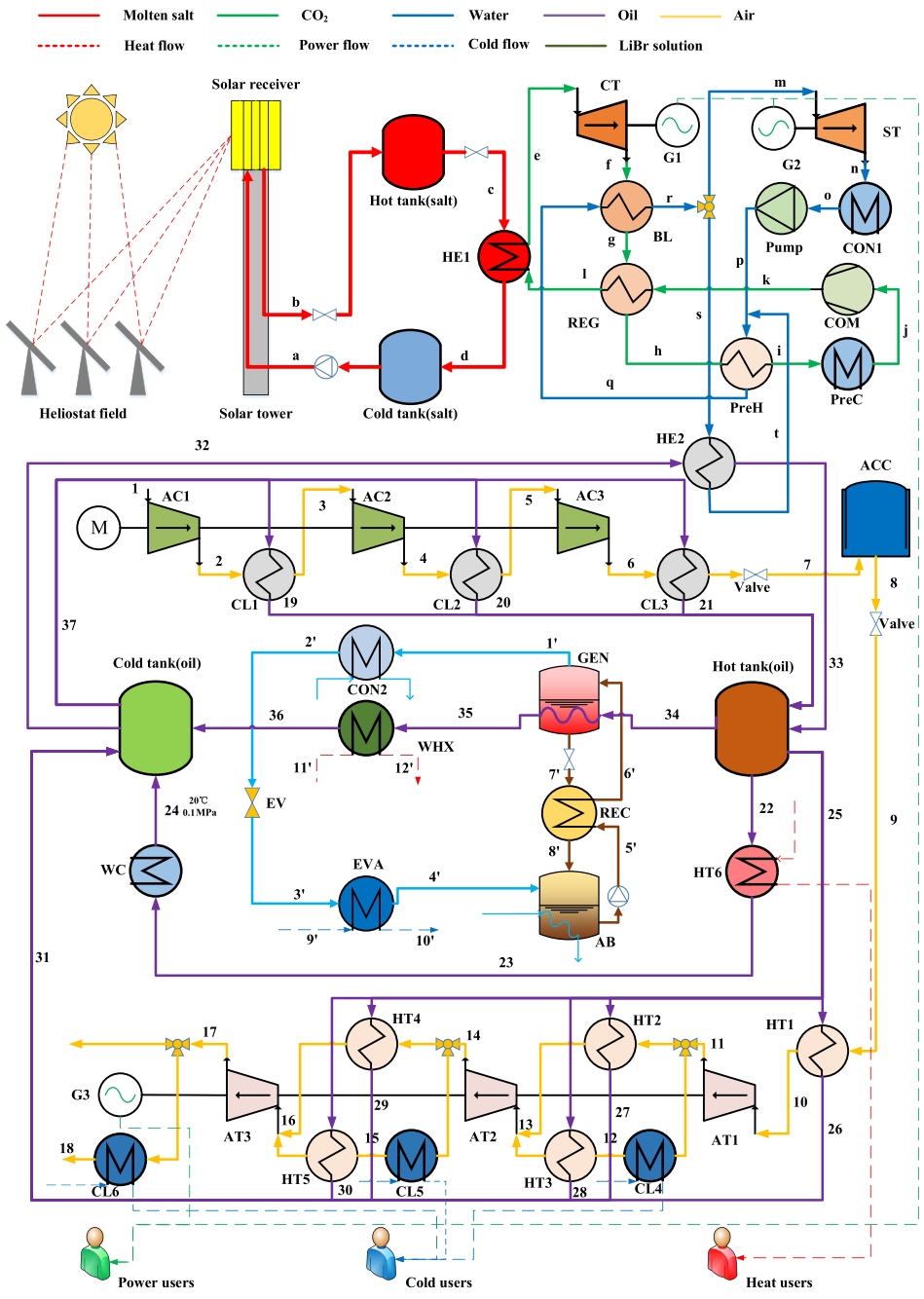

Figure 4. Power station 3 system schematic.

2.2. Power Station 2. The steam generated by BL in Power Station 1 is more than the steam required by ST, and there is waste heat in the high-temperature steam that can be recovered, providing a heat load for the system. Power Station 2 adds a waste heat recovery device on the basis of Power Station 1.[18] The system schematic diagram is shown in Figure 3. Compared with power station 1, the system adds a three-way valve after BL. A part of steam enters the steam turbine to work, and the excess steam flows into the waste heat recovery (WHR) to provide a heat load for the system.

Power generation cycle (e−t): Low-temperature and low-pressure (32 °C, 7.5 MPa) CO_2 enters the COM and pressurizes to 25 MPa. The compressed CO_2 flows through the REG for heat exchange and temperature rise, enters the heat exchanger for heating to 550 °C, and then enters the CT for expansion and work. The heat source of BL is high-temperature and high-pressure CO_2 (393.15 °C, 7.5 MPa), which heats the steam from PreH. After heating, the high-temperature and high-pressure steam enters the steam turbine for work and the excess steam flows into the WHR to provide heating load for the system and then enters the condenser together with the exhaust gas from the steam turbine to complete the cycle.

2.3. Power Station 3. Power Station 3 introduces wind energy on the premise of utilizing solar energy in the SPT. Power Station 3 introduces CAES and AR based on Power Station 2. Compressed air energy storage can be used to absorb wind power. In order to achieve higher cycle efficiency and heat utilization, compressed air energy storage typically adopts the "multistage compression, interstage cooling" and "multistage

https://doi.org/10.1021/acsomega.3c03401
ACS Omega 2023, 8, 42126−42143

expansion, interstage reheat" modes.[19] AR can absorb excess heat energy from the system to provide a cooling load.

The system schematic diagram is shown in Figure 4. The workflow of CAES and AR is as follows:

a. The electrical energy consumed by the three compressors is mainly provided by wind power generation. During this process, the generated high-pressure air (state 7) is stored in the ACC and the compression heat generated during the operation of the three compressors is collected by hot oil (state 37) from the cold tank. After absorbing the compression heat, the hot oil (state 21) mixed together from the three cooler outlets is stored in the hot tank. The ACC inlet is equipped with a valve to ensure that the compressor operates at a constant back pressure at the design point and improve the service life of the compressor.[20]

b. The cogeneration system operates in discharge mode at peak power consumption. The stored air (state 8) is extracted from the ACC and then adjusted to a constant pressure (state 9) by flowing through the valve. The compressed air first enters HT1 for preheating by the hot oil in the hot tank and then enters air turbine 1 (AT1) for expansion and power generation. Part of the low-temperature air from AT1 enters AT2 after being heated in HT2, and the other part of the low-temperature air provides cooling load for the system through cooler 4 (CL4) heat exchange, and then enters HT3 for heating (state 12), and finally enters AT2 for expansion power generation.[20] The working process of HT4, HT5, CL5, CL6, and AT3 is similar to that of the above components, so it will not be repeated. At the same time, high-temperature hot oil is divided into three parts. Part of the hot oil (state 25) is coupled with the compressed air to generate electricity, part of the hot oil (state 22) directly enters HT6 to provide heating load for the system and then flows directly back to the hot oil cooling tank after being cooled by the water cooler (WC), and part of the hot oil (state 34) is used to provide heat source for absorption refrigeration. The low-temperature hot oil (state 32) in the cold tank enters the heat exchanger and exchanges heat with the high-temperature water vapor flowing from the BL to provide the hot oil for the hot tank.

c. The heat supply of the absorption refrigeration cycle mainly depends on the compressor compression heat absorbed in the hot oil tank and the steam waste heat recovered by HE2. The hot oil provides heat for the generator (GEN) (state 34), evaporates the water of lithium bromide solution, and improves the solution concentration. The evaporated steam enters condenser 2 (CON2) (state 1′) for cooling, depressurizes through the EV, and finally enters evaporator (EVA) (state 3′) for evaporation and heat absorption, taking away the heat of the refrigerant water, achieving the purpose of refrigeration. The high-temperature concentrated lithium bromide solution in the GEN enters the recooler (REC) (state 7′) to heat the low-temperature solution in the absorber and then flows into the absorber. The dilute solution in the absorber (AB) flows into the GEN (state 6′) after being heated by the REC to complete the cycle.[21]

3. MATHEMATICAL MODEL

In order to analyze the system and make assumptions about the thermodynamic analysis process, this work makes the following simplification:

a. The scheduling period of the four examples in this paper is 1 day, which is divided into 24 periods, and the length of the period is 1 h. Within a single period of time, environmental factors remain stable.[22]
b. The efficiency of the equipment used in the system is constant during the working process. In a single period of time, the user load (cooling, heating, and power loads) demand and weather conditions (such as ambient temperature and wind speed) are constant and the system is analyzed under a steady state.[23]
c. The pressure loss of gas in the pipeline and heat exchanger is ignored.
d. ACC selects the constant temperature model.[24]
e. The state of evaporator and condenser outlet is saturated steam and saturated liquid, respectively.[25]

The control equation and calculation formula of each part of the system are as follows.

3.1. Latin Hypercube Sampling Scene Generation and Reduction. This review considers the uncertainty of wind power and obtains 10 sets of high-probability wind power output curves through scenario generation and reduction methods to reduce the impact of renewable energy volatility on the system. Among them, 1000 wind power output scenarios that follow probability distribution constraints are generated through Latin hypercube sampling and the scene reduction technique of simultaneous backward reduction (SBR) considering the Kantorovich distance is used to reduce it to 10 scenes. The specific steps are referred to in ref 26. The treatment of solar uncertainty is similar to that of wind power and is not repeated in this section.

In the day-ahead dispatching, the wind power output and direct normal irradiance (DNI) curve are described as

$$P_{\mathrm{w}}(t) = \sum_{S=1}^{10} P_{\mathrm{w},s}(t)\cdot\rho_{s,\mathrm{w}} \tag{1}$$

$$\mathrm{DNI}(t) = \sum_{S=1}^{10} \mathrm{DNI}_{s}(t)\cdot\rho_{s,\mathrm{DNI}} \tag{2}$$

$$E_{\mathrm{wind}}(t) \le P_{\mathrm{w}}(t) \tag{3}$$

Among them, $P_{\mathrm{w}}(t)$is the power generation of wind energy during time t; $P_{\mathrm{w},s}(t)$is the power generation of wind energy in time period t under scenario s; $\rho_{s,\mathrm{w}}$ and $\rho_{s,\mathrm{DNI}}$ are the probabilities of wind and solar scenario s occurring, respectively; and DNI is similar to wind power, so it will not be repeated.

3.2. Heliostat Field and Receiver. The heliostat field can centrally reflect solar energy onto the receiver, and the specific calculation is as follows:

The energy delivered by solar energy to the heliostat field is $Q_{\mathrm{hel,in}}$, which can be expressed by the following formula:

$$Q_{\mathrm{hel,in}} = \mathrm{DNI}\times A_{\mathrm{h}} \tag{4}$$

$$A_{\mathrm{h}} = \sum_{i=1}^{N_{\mathrm{h}}} L_{\mathrm{h}}\times W_{\mathrm{h}} \tag{5}$$

$A_{\mathrm{h}}$is the total area of the heliostat field.

https://doi.org/10.1021/acsomega.3c03401
ACS Omega 2023, 8, 42126−42143

$Q_{hel,out}$represents the output energy of the heliostat field (total solar energy projected from the heliostat field to the receiver aperture).

$$Q_{hel,out} = Q_{hel,in} \times \eta_{hel} \tag{6}$$

$\eta_{hel}$is the overall optical efficiency of the heliostat field.

The energy conservation formula of the solar receiver is

$$Q_{rec,in} = Q_{rec,out} + Q_{rec,ref} + Q_{rec,conv} + Q_{rec,rad} + Q_{rec,cond} \tag{7}$$

$Q_{rec,in}$is the input energy of the solar receiver, equal to the output energy of the heliostat field $Q_{hel,out}$. $Q_{rec,out}$is the energy transferred from solar energy to molten salt, expressed as

$$Q_{rec,out} = m_s(h_{s,b} - h_{s,a}) \tag{8}$$

where m_s is the mass flow of molten salt in the receiving pipe. $h_{s,a}$ and $h_{s,b}$ are the enthalpy of molten salt at the inlet and outlet of the receiver, respectively.[6]

$Q_{rec,cond}$ is the heat loss conducted by the receiver, which can be ignored under the condition of ensuring good insulation. The heat loss caused by convection is calculated as follows:

$$Q_{rec,conv} = \overline{h} \cdot A \cdot (t_{w,out} - t_0) \tag{9}$$

where the mixed convection heat transfer coefficient $\overline{h}$ can be obtained in ref 22.

The radiation loss of the receiver can be calculated as

$$Q_{rec,rad} = A_{rec}\varepsilon_{rec}\sigma(T_{w,out}^4 - T_{am}^4) \tag{10}$$

where ε_{rec} is the emissivity of the receiver.

The reflection loss of the receiver can be calculated as

$$Q_{rec,ref} = (1 - \varphi_{rec})Q_{rec,in} \tag{11}$$

where $\varphi_{rec}$is the absorptivity of the receiver.

3.3. Thermal Energy Storage Model. *3.3.1. Molten Salt Heat Storage.* Solar power generation has problems of volatility and intermittency, and the introduction of energy storage technology can stabilize fluctuations and ensure stable operation of the system. When the solar energy is sufficient, the molten salt is heated by the receiver to a high-temperature molten salt, which enters a cascade cycle for heat exchange. The excess molten salt will be stored in a hot tank; when the solar energy fluctuates, the molten salt in the heat tank is used to maintain the operation of the cascade cycle. This system uses cold and hot double molten salt tanks, and molten salt is composed of 60% $NaNO_3$ and 40% KNO_3. It is assumed that the molten salt storage tank has an excellent thermal insulation performance, ignoring heat loss. The molten salt reserves in the molten salt heat storage tank can be expressed by the following formula:[27]

$$C_{hot,salt}(t) = C_{hot,salt}(t-1) + m_{rec}(t) - \sum_{i=1}^{n} m_k(t) \tag{12}$$

$$C_{cold,salt}(t) = C_{cold,salt}(t-1) - m_{rec}(t) + \sum_{i=1}^{n} m_k(t) \tag{13}$$

where $C_{hot,salt}(t)/C_{cold,salt}(t)$ is the remaining reserve of molten salt in the high/low-temperature molten salt tank during the period t and $m_k(t)$ is the amount of molten salt at high temperature required by the device k to achieve the required heat exchange during the t period.

The inlet and outlet flows of the molten salt tank should meet the upper and lower limit constraints and climbing constraints:

$$\begin{cases} i_k(t)g_{k,min} \le g_k(t) \le i_k(t)g_{k,max} \\ g_{k,low} \le g_k(t+1) - g_k(t) \le g_{k,up} \end{cases} \tag{14}$$

where $i_k(t)$ is the status flag bit of equipment k in the t period, 0 is stop, and 1 is operation; $g_{k,max}/g_{k,min}$ is the maximum/minimum gear of equipment k; and $g_{k,low}/g_{k,up}$ is the lower/upper limit of the climbing rate of equipment k.

The remaining reserves of the high-temperature molten salt tank should meet the following relationship:

$$\begin{cases} C_{hot,salt}^{min} \le C_{hot,salt}(t) \le C_{hot,salt}^{max} \\ C_{hot,salt}^{low} \le C_{hot,salt}(24) - C_{hot,salt}(1) \le C_{hot,salt}^{up} \end{cases} \tag{15}$$

where $C_{hot,salt}^{min}/C_{hot,salt}^{max}$ is the lower/upper limit of the remaining reserves of the high-temperature molten salt tank; $C_{hot,salt}^{low}/C_{hot,salt}^{up}$ is the lower/upper limit of the ramp rate of the remaining reserves of the high-temperature molten salt tank.[28] The model of the low-temperature molten salt tank is the same as that of the high-temperature molten salt tank, so it will not be described again.

3.3.2. Heat Transfer Oil Heat Storage. The mathematical model of oil heat storage heat transfer is similar to that of molten salt heat storage. See Section 10 for details.

3.4. Photothermal Power Generation System Considering CAES. *3.4.1. Thermodynamic Model of the Power Generation Cycle.* The cascaded S-CO_2 Brayton steam Rankine cycle has a more compact layout than the S-CO_2 Brayton cycle.[17] A simple Brayton cycle consists of a compressor, turbine, heat exchanger, and reheater. The system configuration of a cascade cycle is more complex than that of a simple Brayton cycle, adding boilers, preheaters, steam turbines, pumps, and condensers.

Simple Breton cycle efficiency:

$$\eta = \frac{W_{CT} - W_{COM}}{Q_c} \tag{16}$$

Cascade cycle efficiency:

$$\eta = \frac{W_{CT} - W_{COM} + W_{ST} - W_{Pump}}{Q_c} \tag{17}$$

The mass flow of steam can be obtained by the following formula:

$$m_s = \frac{h_f - h_g + h_h - h_i}{h_m - h_k} \tag{18}$$

h_f, h_g, h_h, h_i, h_m, and h_k are the enthalpy of the fluid at different positions.

3.4.2. Compressor and Expander in the Cascaded S-CO_2 Brayton-Steam Rankine Cycle. The energy balance of the compressor in the S-CO_2 Brayton cycle is[17]

$$\eta_c = (h_{ks} - h_j) / (h_k - h_j) \tag{19}$$

$$W_{COM} = m_{COM}(h_k - h_j) \tag{20}$$

The energy balance of expander in the S-CO2 Brayton cycle is

$$\eta_t = (h_e - h_f) / (h_{es} - h_f) \tag{21}$$

https://doi.org/10.1021/acsomega.3c03401
ACS Omega 2023, 8, 42126−42143

$$W_{CT} = m_{CT}(h_e - h_f) \tag{22}$$

The energy balance of the pump in the steam Rankine cycle is

$$W_{Pump} = m_{Pump}(h_p - h_o) \tag{23}$$

The energy balance of steam turbine in steam Rankine cycle is

$$\eta_{ST} = (h_m - h_n) / (h_m - h_{ns}) \tag{24}$$

$$W_{ST} = m_s(h_m - h_n) \tag{25}$$

3.4.3. Heat Exchanger. Heat exchanger is energy-saving equipment that can transfer heat between materials between two or more fluids at different temperatures. It is used to transfer heat from the fluid with a higher temperature to the fluid with a lower temperature. In the four cases in this paper, the heat exchanger is used as heater, cooler, condenser, evaporator, etc.[29]

The energy balance equation of the heat exchanger is

$$m_h(h_{h,in} - h_{h,out}) = m_c(h_{c,in} - h_{c,out}) \tag{26}$$

where m_h is the mass flow of hot fluid; m_c is the mass flow of cold fluid; $h_{h,in}/h_{h,out}/h_{c,in}/h_{c,out}$ are the inlet/outlet enthalpy of hot/cold fluid, respectively.[30]

3.4.4. Compressed Air Energy Storage. The three-stage compressor uses the same pressure ratio, which can allow the compressor to operate with low power consumption. The compressor pressure ratio can be written as

$$C_{r,AC} = \frac{P_2}{P_1} = \frac{P_3}{P_4} = \frac{P_6}{P_5} \tag{27}$$

The isentropic efficiency and power consumption of compressors at all levels are

$$\eta_{AC} = \frac{h_{out,x} - h_{in}}{h_{out} - h_{in}} \tag{28}$$

$$W'_{AC,i} = m'_{air,ch}\frac{C_p T_{in,i}}{\eta_{AC}}[(C_{r,AC})^{k-1/k} - 1] \tag{29}$$

where k is the isentropic index; i, ch, and x are the number of compressors, the number of intake air, and the number of isentropic processes, respectively.[31]

The total power consumption of the compressor is

$$W'_{AC} = \sum_{i=1}^{3} W'_{AC,i} \tag{30}$$

For each cooler, the compression heat absorbed by the heat transfer oil can be calculated as

$$Q'_{CL} = m'_{air,ch}(h_{air,in} - h_{air,out}) = m'_{oil}(h_{oil,out} - h_{oil,in}) \tag{31}$$

Two valves are arranged at the inlet and outlet of the ACC to keep the inlet and exhaust pressure constant. Turbomachinery operating under constant pressure can improve safety.[32] The air flow through the valve is considered as a constant enthalpy process:

$$h_9 = h_8 \tag{32}$$

For each heater, the energy balance equation of heat exchange between air and heat transfer oil can be expressed as

$$Q'_{HT} = m'_{air,di}(h_{air,out} - h_{air,in}) = m'_{oil}(h_{oil,in} - h_{oil,out}) \tag{33}$$

where subscript di represents the discharge process.

For each air turbine, the expansion ratio is

$$C_{r,AT} = \frac{P_{10}}{P_{11}} = \frac{P_{13}}{P_{14}} = \frac{P_{16}}{P_{17}} \tag{34}$$

In the expansion process, the isentropic efficiency and output power of the three air turbines are

$$\eta_{AT} = \frac{h_{in} - h_{out}}{h_{in} - h_{out,x}} \tag{35}$$

$$W'_{AT,i} = m'_{air,di}c_p T_{in,i}[1 - (C_{r,AC})^{k-1/k}] \tag{36}$$

The total power output of the air turbine can be expressed as

$$W'_{AT} = \sum_{i=1}^{3} W'_{AT,i} \tag{37}$$

Low-temperature turbine exhaust can provide cooling load for users, and its cooling energy can be calculated as

$$Q'_{Cooling} = m'_{air,di}c_p(T_0 - T_{18}) \tag{38}$$

Subscript 0 indicates environmental conditions.

The modeling process of air accumulator (ACC) is similar to that of a molten salt tank. In the CAES cycle, ACC is used to replace the underground salt cavern for further promotion. The mass equation of the ACC is as follows:

$$C_{ACC,tank}(t) = C_{ACC,tank}(t\text{-}1) + m_{AC}(t) - m_{AT}(t) \tag{39}$$

where $C_{ACC,\,tan\,k}(t)$ is the residual capacity of the ACC during period t.

The inlet volume of the ACC shall meet the upper and lower limit constraints and climbing constraints:

$$\begin{cases} i_k(t)g_{k,min} \le g_k(t) \le i_k(t)g_{k,max} \\ g_{k,low} \le g_k(t+1) - g_k(t) \le g_{k,up} \end{cases} \tag{40}$$

where $i_k(t)$ is the status flag bit of equipment k in the t period, 0 is stop, and 1 is operation; $g_{k,max}/g_{k,min}$ is the maximum/minimum gear of equipment k; and $g_{k,low}/g_{k,up}$ is the lower/higher limit of the climbing rate of equipment k.

3.4.5. Thermal Efficiency. The overall thermal efficiency of the S-CO_2 Brayton cycle and compressed air energy storage is defined as

$$\eta_{SC-ACES} = \frac{\sum_{t=1}^{24} E_{CT}(t) + \sum_{t=1}^{24} E_{ST}(t)}{\sum_{t=1}^{24}\sum_{k=1}^{n} m_k(t) + \sum_{t=1}^{24} E_{COM}(t) + \sum_{t=1}^{24} E_{pump}(t)} \tag{41}$$

3.5. Absorption Refrigeration. The heat supply of the AR cycle mainly depends on the compressor compression heat absorbed in the heat transfer oil tank and the steam waste heat recovered by HE2. In the AR cycle, the heat transfer oil releases heat into the lithium bromide solution in the generator. Then, the working medium was converted into concentrated lithium bromide solution and steam. The water vapor in the generator

https://doi.org/10.1021/acsomega.3c03401
ACS Omega 2023, 8, 42126−42143

enters the condenser and condenses into water, which is depressurized by the expansion valve and enters the evaporator for evaporation and heat absorption, thus providing cooling load. Finally, water enters the absorber to reduce the concentration of the solution. This section refers to ref[21], in which the calculation details of pressure, entropy, and enthalpy in the system flow are shown in Section 33.

3.6. Electric Boiler. As a kind of energy conversion equipment with an electric-thermal coupling function, EB has high electric-thermal conversion efficiency. In addition, the EB can also promote the decoupling control of the cogeneration unit; in other words, the thermal output of the EB can reduce the heating pressure of the cogeneration unit. The EB consumes electric energy for heat production, and its energy equation is

$$Q_{EB} = W_{EB} \times COP_{EB} \tag{42}$$

where Q_{EB} is the heat output of the electric boiler; $W_{EB}$is the electric energy consumed by the electric boiler; and $COP_{EB}$is the heat-electricity conversion efficiency of the electric boiler.

The constraints to be met are

$$\begin{cases} i_{EB}(t)W_{EB,min} \le W_{EB}(t) \le i_{EB}(t)W_{EB,max} \\ W_{EB,low} \le W_{EB}(t+1) - W_{EB}(t) \le W_{EB,up} \end{cases} \tag{43}$$

where $W_{EB,min}/W_{EB,max}$ is the upper/lower limit of power consumption of electric boiler; $i_{EB}(t)$ is the status flag bit of the electric boiler in time period t, 0 is stop, and 1 is running; and $W_{EB,up}/W_{EB,low}$ is the upper/lower limit of the ramp rate of electric boiler power consumption.[33]

3.7. Electric Chiller. The EC is driven by electricity, and its cooling capacity is

$$Q_{EC} = W_{EC} \times COP_{EC} \tag{44}$$

where $W_{EC}$is the electric energy consumed by the EC, in kW; COP_{EC} is the performance coefficient of the EC, which is 3.0.

The constraints to be met are

$$\begin{cases} i_{EC}(t)W_{EC,min} \le W_{EC}(t) \le i_{EC}(t)W_{EC,max} \\ W_{EC,low} \le W_{EC}(t+1) - W_{EC}(t) \le W_{EC,up} \end{cases} \tag{45}$$

where $W_{EC,max}/W_{EC,min}$ is the upper/lower limit of the power consumption of the EC; $i_{EC}(t)$ is the status flag bit of the EC in the t period, 0 is stop, and 1 is operation; and $W_{EC,up}/W_{EC,low}$ is the upper/lower limit of power consumption ramp rate of EC.[34]

3.8. Waste Heat Recovery. There is waste heat from the steam heated by the boiler that can be used. Waste heat recovery (WHR) can be used to recover waste heat to increase the heating load and improve energy utilization efficiency. This paper does not specifically analyze the WHR but considers only the heat recovered. The energy equation is as follows:[35]

$$Q_{WHR}(t) = m_{WHR}(t)(h_{WHR,in} - h_{WHR,out}) \tag{46}$$

where $Q_{WHR}(t)$is the heat recovered by the WHR in the t period; $m_{WHR}(t)$ is the mass flow of the steam of the medium-temperature heat source; and $h_{WHR,in}/h_{WHR,out}$is the inlet enthalpy/outlet enthalpy of medium-temperature heat source steam.

4. ECONOMIC DISPATCH MODEL

The integrated energy system established in this paper considers CSP, CAES, and AR and formulates the optimal output plan of each piece of equipment and the system day-ahead scheduling plan. The capacity of molten salt storage tanks, ACC, and heat transfer oil tanks as well as the balance of cold, heat, and electrical loads is analyzed. See Section 6for specific mathematical models of each component. The energy flow of power stations 1 and 2 is similar to that of power station 3, so the analysis is conducted for power station 3.

4.1. Objective Function. The day-ahead optimization model of the CCHP system based on CSP, CAES, and AR is established in this paper. The objective function is to minimize the economic cost, which means that the power purchase cost of large power grids is minimal:

$$F = \sum_{t=1}^{24} E_g(t) \times \tau_g(t) \tag{47}$$

where $E_g(t)$ is the power purchased by the power grid in the t period; $\tau_g(t)$ is the electricity price of the power grid in the t period, which is different in different periods.

4.2. Constraint Condition. In addition to the constraints of the mathematical model established in Section 6, the system also needs to meet the constraints of cold, hot, and electric power balance, the interactive power constraints of the large power grid, and reserve capacity constraints.[36]

Cold power balance:

$$Q_{AR}(t) + Q_{EC}(t) + Q_{CL}(t) = Co(t) \tag{48}$$

Hot power balance:

$$Q_{EB}(t) + Q_{WHR}(t) + Q_{HT}(t) = Ho(t) \tag{49}$$

Electric power balance:

$$\begin{aligned} &E_g(t) + E_{AT}(t) + E_{CT}(t) \\ &+E_{ST}(t) - E_{COM}(t) - E_{Pump}(t) \\ &-E_{AC}(t) + E_{Wind}(t) = \\ &E_{EB}(t) + E_{EC}(t) + E(t) \end{aligned} \tag{50}$$

Interaction power constraint of a large power grid:

$$\begin{cases} E_{g,min} \le E_g(t) \le E_{g,max} \\ E_{g,low} \le E_g(t+1) - E_g(t) \le E_{g,up} \end{cases} \tag{51}$$

where $Co(t)/Ho(t)/E(t)$ is the user's cooling/heating/electric load demand; $E_{g,max}/E_{g,min}$ is the upper and lower limit of interactive power of large power grid; and $E_{g,up}/E_{g,low}$ is the upper and lower limits of the ramp rate of the large power grid.

The mathematical model established in this paper is the day-ahead scheduling model. In actual operation, the cooling, heating, power load, wind power output, and DNI curve required by users deviate from the predicted value. In response to such issues, consider the backup constraint of the cooling, heating, and power load capacity to ensure that decision-making institutions can adjust the output of equipment, thereby ensuring stable cooling, heating, and power supply for users.[37]

The capacity constraints for electrical backup are

$$\begin{aligned} R_{up}(t) &\le \sum_{i=1}^{M} E_{max,i}(t) - E_i(t) \\ R_{down}(t) &\le \sum_{i=1}^{M} E_i(t) - E_{min,i}(t) \end{aligned} \tag{52}$$

https://doi.org/10.1021/acsomega.3c03401
ACS Omega 2023, 8, 42126−42143

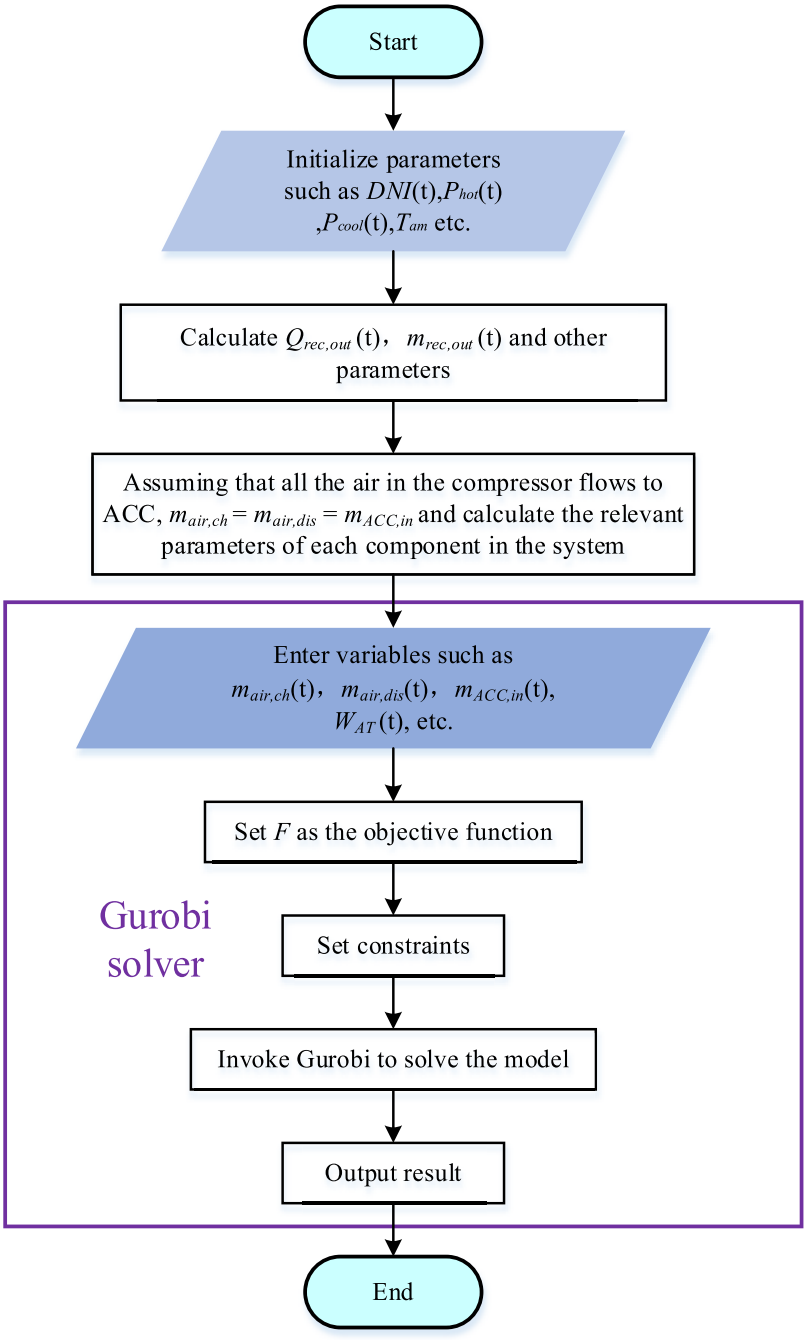

Figure 5. Solution process of power station 3 operation optimization.

where $R_{up}(t)/R_{down}(t)$ is the upper and lower limits of the electrical backup constraint; and $E_i(t)$ is the output of device i during time t; $E_{max,i}(t)/E_{min,i}(t)$ is the maximum/minimum output of device i during time t. The constraints of cold and heat backup are similar to those of electric backup and will not be elaborated in this article.

4.3. Model Solving. The system model established in this paper is a mixed-integer linear programming problem involving many variables. A thermodynamic analysis of the established system model is conducted. The thermodynamic properties of the working fluid are obtained by using REFPROP 9.1 software, and the system simulation is completed by self-coding in the mathematical software MATLAB. The commercial optimization software Gurobi solver is called YALMIP to solve the model. The solution flowchart is shown in Figure 5.

5. EXAMPLE ANALYSIS

Based on the data of typical days and combined with practical engineering construction examples, this work considers the economic cost of the system and energy utilization. The equipment output and cooling, heating, and electrical load balance in CCHP is studied, and the effectiveness of this study through simulation analysis is demonstrated. The scheduling period of the example is 24 h, and the length of a single period is 1 h.

5.1. Basic Data. This article refers to the typical daily cooling, heating, and electricity load demand curves in ref 38 and

https://doi.org/10.1021/acsomega.3c03401
ACS Omega 2023, 8, 42126−42143

the 24 h time-of-use electricity price curve in ref 39, used to construct the basic environmental data and related parameters of the system. The wind power generation prediction curve and 24 h DNI prediction curve in this article are generated from a large number of scenarios using Latin hypercube sampling and then obtained by considering the synchronous backpropagation of Kantorovich distance to eliminate the scenarios. Figure 6 is the prediction curve for wind power generation; Figure 7 is the 24 h DNI prediction curve; Figure 8 shows the typical daily cooling, heating, and power load prediction curves; and Figure 9 is the time-of-use electricity price.

In this paper, the parameters of microsource equipment are set as follows: The initial storage capacity and maximum storage capacity of molten salt are 3600 and 16,200 t, respectively; the

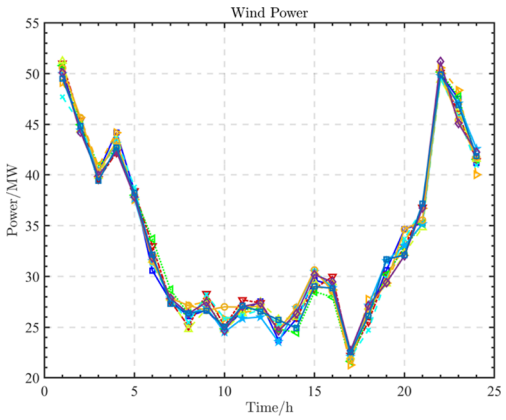

Figure 6. Wind power prediction curve.

initial capacity and maximum capacity of the heat transfer oil tank are 900 and 1800 t, respectively; the initial storage capacity and maximum storage capacity of ACC are 360 and 1080 t, respectively; and the rated power of EB, EC, and AR is 30, 20,

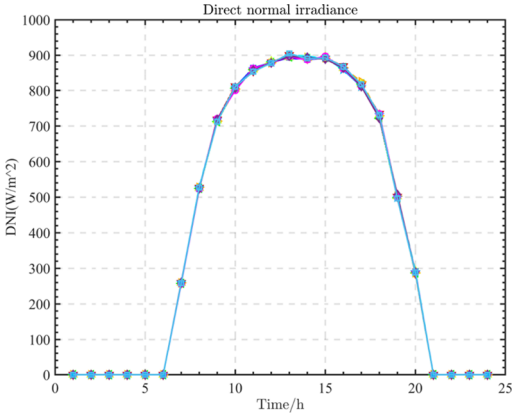

Figure 7. DNI prediction curve.

and 5 MW, respectively. The unit equipment correlation coefficients and system environmental parameters are shown in Appendix C, Tables 4 and 5.

In order to demonstrate the effectiveness of the system, this article sets up four cases based on the actual situation, as follows:

Case 1: Conventional CCHP system without considering the power station.

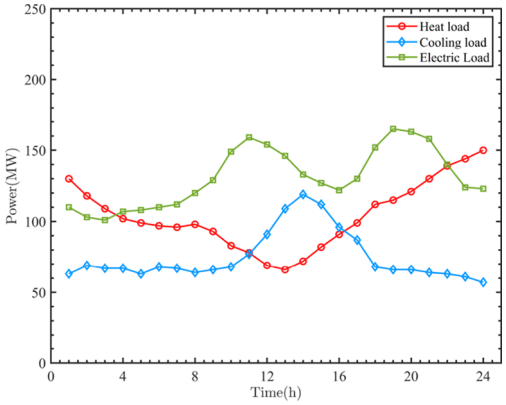

Figure 8. Typical daily cooling, heating, and power load prediction curves.

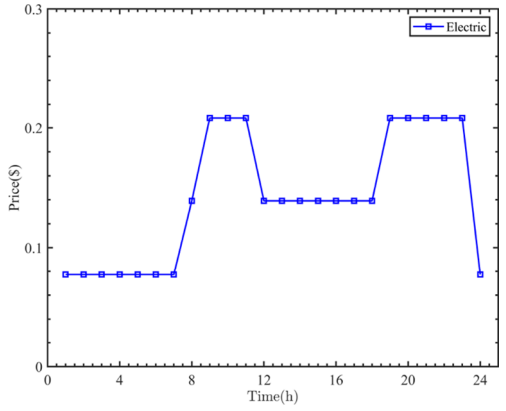

Figure 9. Time-of-use electricity price ($/kW·h).

Case 2: The system is shown in Figure 1, using power station 1, and the layout of power station 1 is shown in Figure 2.

Case 3: The system is shown in Figure 1, using power station 2, and the layout of power station 2 is shown in Figure 3.

Case 4: The system is shown in Figure 1, using power station 3, and the layout of power station 3 is shown in Figure 4. The energy flow relationship of power station 3 is shown in Table 3.

5.2. Optimization Results and Analysis of Power Station 1. The electric load balances of cases 1 and 2 are shown in Figure 10a and b, respectively. The cooling and heating loads for case 1 are provided by EC and EB, respectively. It can be seen from Figure 10a that the peak output of EC is mainly in periods 12−16 and the peak output of EB is mainly in periods 0−4 and 19−24, The peak of electrical load occurs during periods 9−13 and 18−22. The peak load demand of users leads to high energy supply pressure in large power grids during periods 10−14 and 18−22.

As shown in Figure 10b, after using power station 1 in case 2, the user's load is provided by the large power grid and power station 1. Compared to case 1, the power grid output in case 2 decreased significantly during periods 9−13, 16, and 19−22. Periods 8−11 and 18−23 are peak periods for power purchase prices; during this period, case 2 purchased less electricity from the grid than case 1 and the cost of purchasing electricity in case 2 decreased by 42.26%. The total power supplied by ST to the system in 24 h is 249.37 MW, which is much higher than the

https://doi.org/10.1021/acsomega.3c03401
ACS Omega 2023, 8, 42126−42143

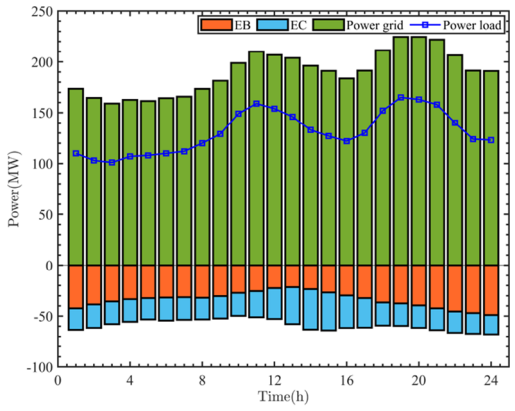

(a) Electric load balance of case 1

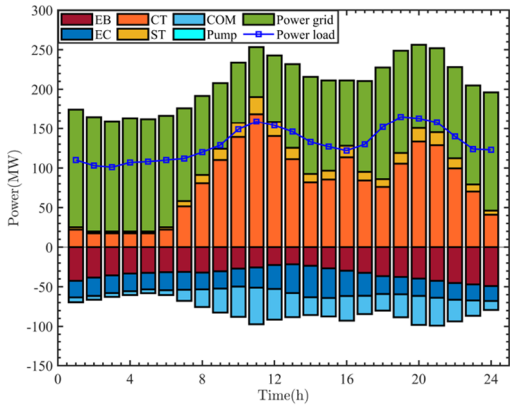

(b) Electric load balance of case 2

Figure 10. Electric load balance of cases 1 and 2.

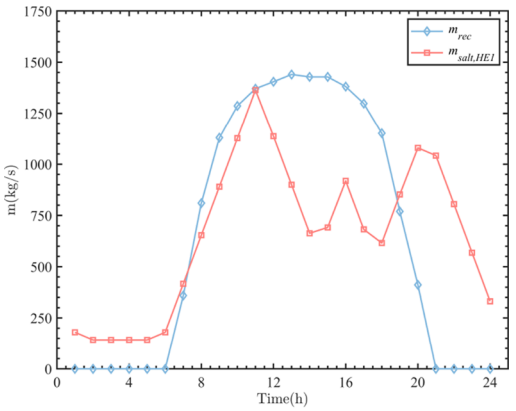

(a) Molten salt flow

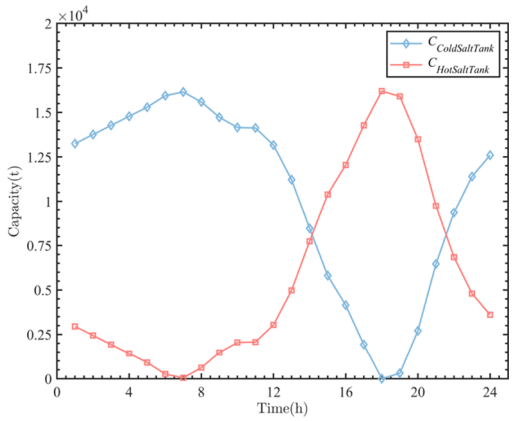

(b) Molten salt tank capacity

Figure 11. Case 2 Heat storage equipment scheduling.

total power consumed by pump of 0.5 MW, indicating that the power output ratio of the steam cycle is high.

The scheduling results of heat storage equipment in case 2 are shown in Figure 11a,b. The molten salt flow in HE1 is positively correlated with the electrical load and also positively correlated with DNI in periods 6−19. The reason for the above relationship is that molten salt is the heat storage medium of the system. The molten salt absorbs heat through the tower collector, and the high-temperature molten salt is stored in the hot tank; with the increase of electric load demand, high-temperature molten salt and low-temperature CO_2 exchange heat, making the working medium CO_2 change into high-temperature and high-pressure state, and enter CT to work, providing electric load to the system. During 14−17, the demand for electric load decreases and the work of CT decreases during this period, so the molten salt flow demand in HE1 is reduced. The capacity of the hot molten salt storage tank is at the maximum in period 18, and the capacity of the cold tank is at the maximum in period 7.

5.3. Optimization Results and Analysis of Power Station 2. The electric load balance of case 3 is shown in Figure 12. In case 3, the output trends of CT and ST are similar, with peak output during the 9−13 and 17−21 periods. In period 5, the CT did not produce power because the high-temperature molten salt was produced when the solar energy was sufficient during the day, and the high-temperature molten salt was consumed when there was no solar energy; during periods 5−7, the molten salt in the hot tank is almost completely consumed. The output of EC and EB is similar to that of case 2. In the

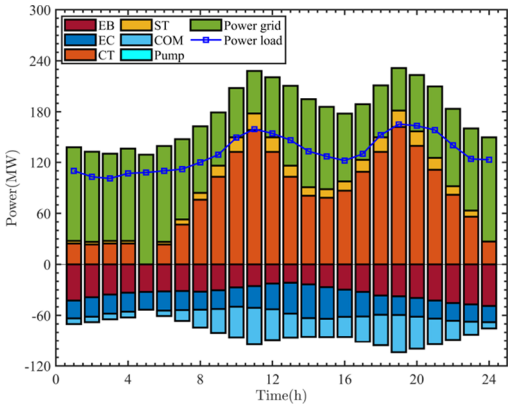

Figure 12. Electric load balance of case 3.

period of high outputs of CT and ST, the power purchased by the system from the grid will be reduced. These periods are also the peak periods of the electric load and electricity price. ST and CT achieved the task of "peak shaving" of the grid power supply, and the system cost of case 3 was reduced by 26.48% compared to case 2.

The heat load balance of case 3 is shown in Figure 13. During the 0−7 period, the high-temperature molten salt generated by sufficient solar energy during the day is gradually consumed and the CT and ST outputs are not significant in the power generation cycle. The heat load of the system is mainly provided by the EB. The WHR provides a heat load of 42.71 MW for the

https://doi.org/10.1021/acsomega.3c03401
ACS Omega 2023, 8, 42126−42143

system during periods 8 and 19−24. Period 19−24 is the peak period of the system's heat load. It can be seen that the WHR can alleviate the heating pressure of the system during the peak period of the heat load.

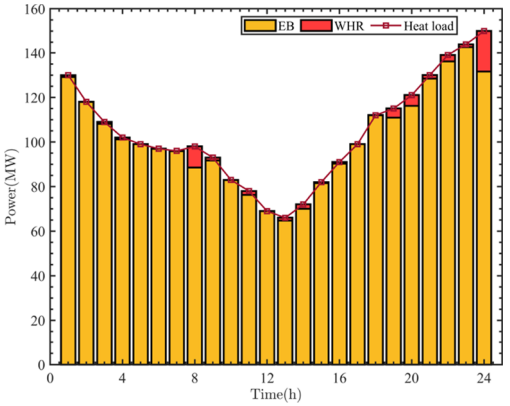

Figure 13. Heat load balance in case 3.

The scheduling results of the heat storage equipment in case 3 are shown in Figure 14a,b. In periods 11 and 19, the CT and ST output is the highest and the HE1 molten salt flow is significantly higher than the other periods. The main reason for the fluctuation of the HE1 molten salt flow curve is related to the electrical and heat loads, where the electrical and heat load demand is small in the 13−17 time period, thus not requiring a lot of power from the CT, and the HE1 molten salt flow decreases. In period 5, the HE1 molten salt flow rate is 0. The capacity of the hot tank is at the maximum value in period 18, and the capacity of cold tank is at the maximum value in period 7.

The steam diversion in case 3 is shown in Figure 15. The steam flow curve in ST is similar to that of the molten salt flow curve in HE1. During the 8, 19−20, and 24 periods, excess steam can be utilized by WHR to provide heat load to the system, which improves the energy efficiency of the system and reduces the economic cost of the system.

5.4. Optimization Results and Analysis of Power Station 3. The power load balance for case 4 is shown in Figure 16a. During the periods of 9−11 and 19−21, the output of CT, ST, and AT was significant. Compared to case 3, case 4 further reduced the system's power purchase from the grid, indicating that the introduction of CAES can participate in the optimization of the entire system as an auxiliary system; the three-stage air turbine power generation in compressed air energy storage can be used to reduce the cost of power purchase and alleviate the pressure on the superior power grid. During periods 0−5 and 22−24, the compressor operates to compress the air and store it in the ACC. AT releases air for work during periods 9−11, 19, and 21 to provide electrical energy to the system. AC consumes a total of 82 MW of wind power at night, while AT provides 54 MW of electricity to the system during peak load periods, indicating that compressed air energy storage can play a role in dissipating wind power and " peak load shifting".

The heat load balance of case 4 is shown in Figure 16b. During the unloading process of the heat transfer oil tank, the heat transfer oil carrying a large amount of compressed heat is divided into three parts. Part of it is sent to the heater to increase the temperature of the high-pressure air entering the air turbine, thereby increasing the power of the air turbine; part of it is used

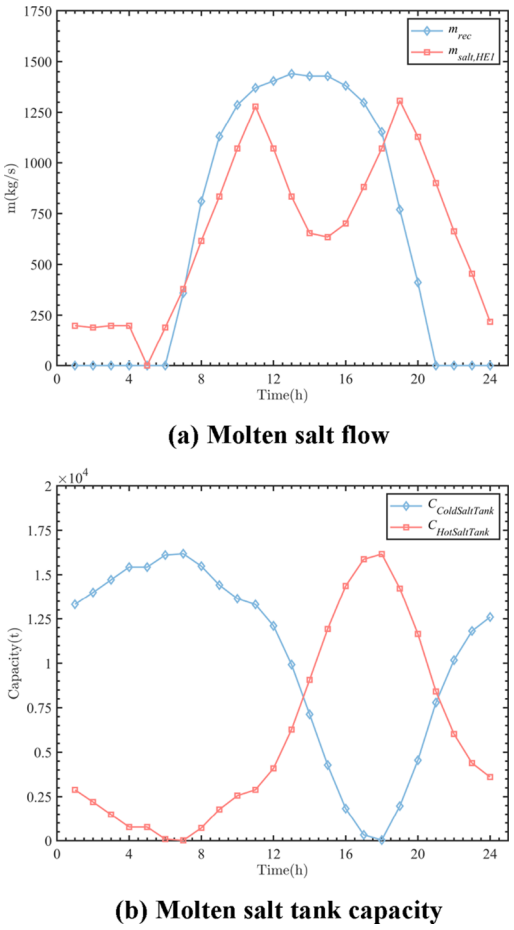

Figure 14. Case 3 Heat storage equipment scheduling.

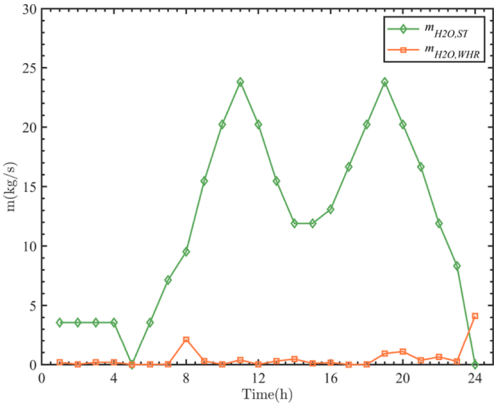

Figure 15. Case 3 Steam diversion situation.

to drive absorption refrigeration to provide heating energy; and part of it provides heat load for the system through HT6. The results show that HT6 provides a total heat load of 246 MW for the system, provide 60 MW thermal load during period 23, and bear 41.67% of the system's thermal load during this period, indicating that introducing compressed air energy storage can improve the heating capacity of the system. While providing heat, HT6 plays a role in balancing the heat transfer oil tank.

The cooling load balance for case 4 is shown in Figure 16c. The cooling load in the system is borne by EC, CL, and AR. The results show that during periods 3, 4, and 23, AR can convert the excess heat energy in the system into 12 MW of cold energy; CL

https://doi.org/10.1021/acsomega.3c03401
ACS Omega 2023, 8, 42126−42143

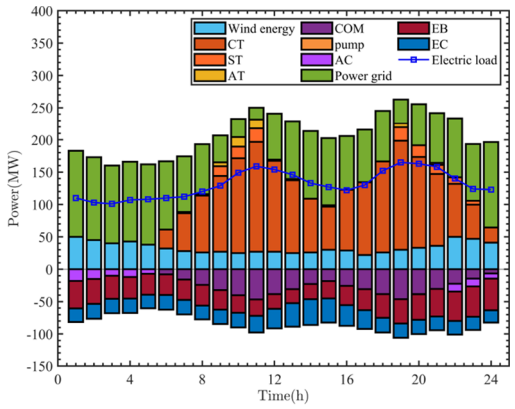

(a) Electric load balance of Case 4

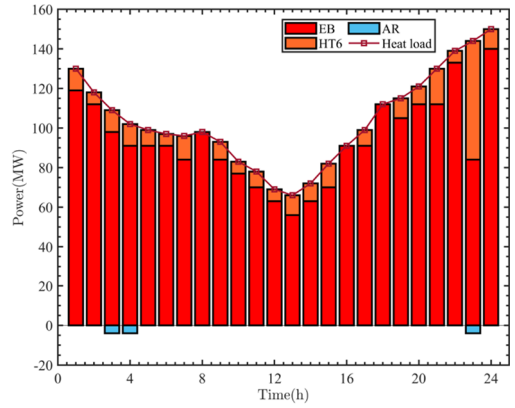

(b) Heating load balance of Case 4

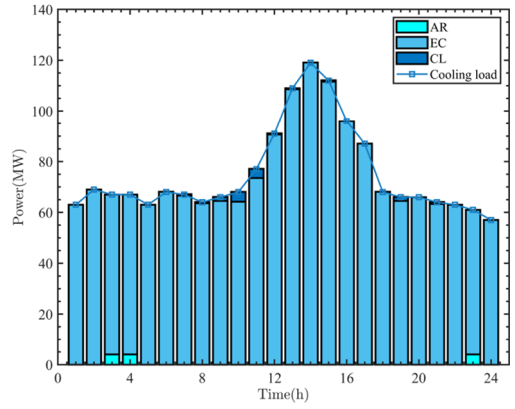

(c) Cooling load balance of Case 4

Figure 16. Electric, heating, and cooling load balance of case 4.

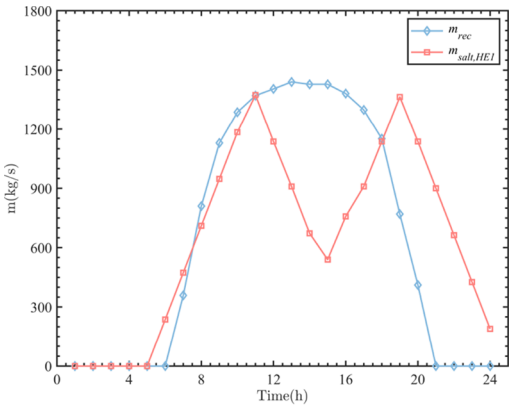

(a) Molten salt flow

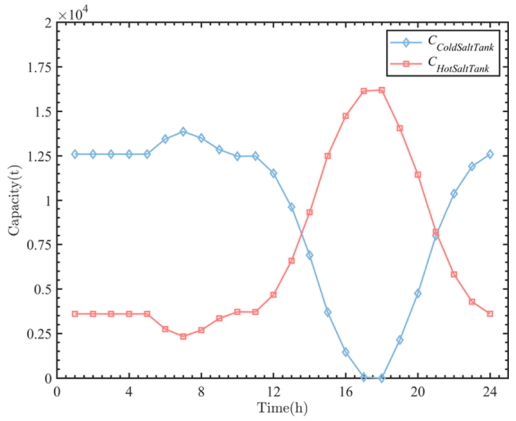

(b) Molten salt tank capacity

Figure 17. Case 4 Heat storage equipment scheduling.

provides a total cooling load of 13.76 MW for the system, indicating that the low-temperature air at the outlet of the tertiary air turbine is utilized by CL4−6.

The scheduling results of hot melt salt energy storage in case 4 are shown in Figure 17a,b, which are similar to the previous case; therefore, it will not be repeated.

The capacity of the ACC in case 4 is shown in Figure 18a. ACC capacity is at the minimum value in period 21 and the maximum value in period 5−6. ACC capacity gradually increases in 0−5 and 21−24 periods and decreases in 8−11 and 18−21 periods, indicating that compressed air storage consumes wind power compressed air during the peak period of wind power generation and releases air to provide power during the peak period of load.

The wind power accommodation in case 4 is shown in Figure 18b,c. CAES can be used for wind power accommodation. In periods 0−5 and 22−24, during periods of high wind power generation at night, the compressor consumes 94 MW of wind power to compress air for energy storage; during peak load periods, the air turbine releases air to provide 54 MW of electrical energy to the system. It can be seen that CAES has a " peak load shifting" effect on the load.

The scheduling results of the heat transfer oil heat storage equipment under case 4 are shown in Figure 19. In case 4, the storage change curve of the heat transfer oil tank is shown in Figure 19a, and the general trend is similar to that of the molten salt storage tank. In case 4, the amplitude and frequency of the flow change curves of each equipment requiring heat transfer oil are relatively large. The main reason is that the compressed air energy storage cycle has the characteristics of combined cooling, heating, and electricity, which can improve the energy supply capacity of the system, but increases the complexity of the overall system operation.

According to the analyses of Figure 15c and Figure 20, it is feasible to use excessive high-temperature heat transfer oil to drive a 5 MW absorption refrigerator. However, the cold load ratio provided by AR is far lower than that of EC. According to the calculation, the accumulated cooling capacity of AR in 24 h is 12 MWH. This is because this paper considers that AR is mainly used to consume excessive heat transfer oil to keep the capacity balance of the oil tank and improve the system economy.

https://doi.org/10.1021/acsomega.3c03401
ACS Omega 2023, 8, 42126−42143

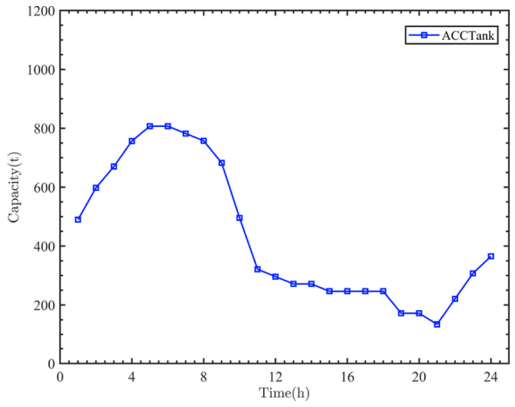

(a) The capacity of ACC

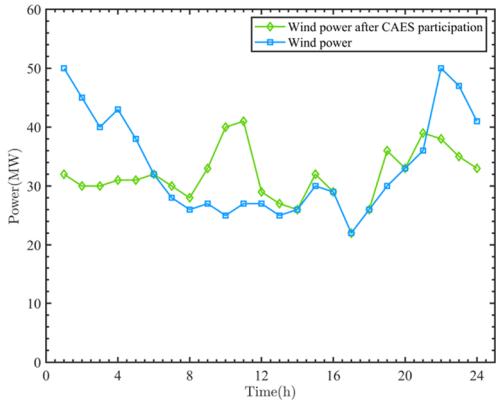

(b)Wind power after CAES participation

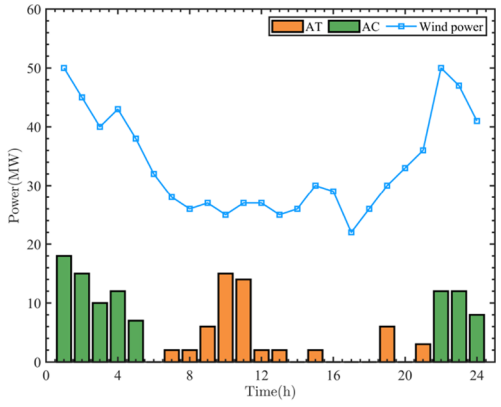

(c) Operation of AT and AC

Figure 18. Case 4 Scheduling of compressed air energy storage.

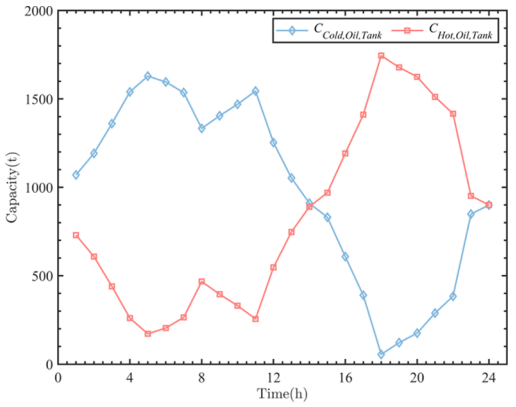

(a) Heat transfer oil tank capacity

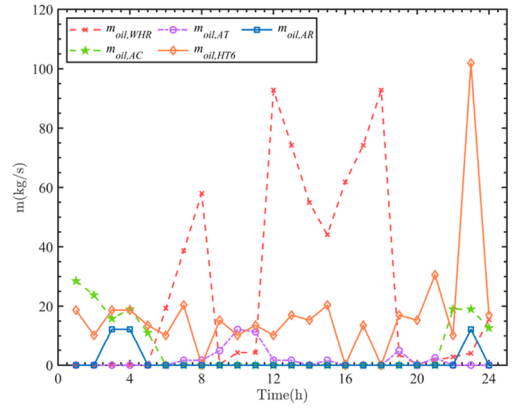

(b) Heat transfer oil flow rate

Figure 19. Case 4 Heat storage equipment scheduling.

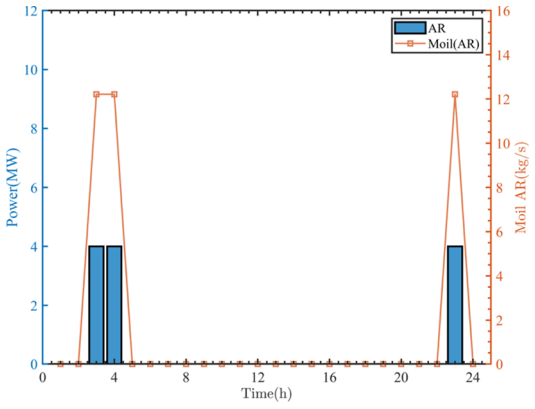

Figure 20. AR scheduling results in case 4.

5.5. Economic Cost Analysis of Each Case. The economic costs of the four cases are listed in Table 1. When power station 1 participates in system optimization, the total operating cost of the system is significantly reduced, which is 42.26% lower than that of conventional CCHP systems. After considering power station 2 in case 3, the system cost decreased by 26.48% compared to case 2. After considering power station 3 in case 4, it decreased by 59.94% compared to case 1. This indicates that considering the combined cooling, heating, and electricity type of power station 4 has higher economic value and the introduction of CSP, CAES, and AR is necessary.

Table 1. Economic Cost of Cases 1−4

case	total cost ($)
1	651924.6
2	376421.8
3	276757.0
4	261136.8

6. RESULTS AND DISCUSSION

This paper proposes a CCHP system based on CSP, CAES, and AR, and its day-ahead scheduling model. The purpose is to

https://doi.org/10.1021/acsomega.3c03401
ACS Omega 2023, 8, 42126−42143

establish power stations based on clean energy; provide users with cooling, heating, and electricity loads; improve the utilization rate of clean energy; and conduct economic analysis on different power stations. Through case analysis, conclusions are drawn:

a The CCHP system composed of CSP, CAES, and AR cycles has the ability to complement multiple energy sources, providing users with stable cooling, heating, and electrical loads.

b Only considering the CSP system can improve the system's economy, reducing the system's operating costs by 42.26%. In addition, considering that thermal energy storage devices can improve the solar energy absorption rate, that is, the absorption rate of solar energy is 81.92%.

c Considering the systems of CSP and CAES not only improves the economy of the system but also improves the absorption rate of wind and solar energy. Among them, the operating cost decreased by 59.94%; the absorption rate of wind energy is 100%, and the absorption rate of solar energy is 99.89%.

d The heat transfer oil circulation achieves waste heat recovery of the system and provides users with a heat load of 246 MW. In addition, AR provides users with a 12 MW cooling load by recovering the heat transfer oil waste heat.

APPENDIX A

Absorption Refrigeration Model

$$X_{\text{strong}} = (49,.,04,+,1,.,125,t_A,-,t_E) / (134,.,65,+,0,.,47,t_A)\text{kgLiBrsolution} \quad (53)$$

$$X_{\text{weak}} = (49,.,04,+,1,.,125,t_G,-,t_C) / (134,.,65,+,0,.,47,t_G)\text{kgLiBrsolution} \quad (54)$$

$$X_{1'} = X_{2'} = X_{3'} = X_{\text{weak}} \quad (55)$$

$$X_{4'} = X_{5'} = X_{6'} = X_{\text{strong}} \quad (56)$$

$$h_A = (A_0,+,A_1,X_{\text{weak}})t_A + 0.5(B_0,+,B_1,X_{\text{weak}})t_A^2 + (D_0,+,D_1,X_{\text{weak}},+,D_2,X_{\text{weak}}^2,+,D_3,X_{\text{weak}}^3) \quad (57)$$

$$h_G = (A_0,+,A_1,X_{\text{strong}})t_G + 0.5(B_0,+,B_1,X_{\text{strong}})t_G^2 + (D_0,+,D_1,X_{\text{strong}},+,D_2,X_{\text{strong}}^2,+,D_3,X_{\text{strong}}^3) \quad (58)$$

$$m_{6'} = X_{1'} / (X_{6'},-,X_{1'}) \quad (59)$$

$$m_{1'} = X_{6'} / (X_{6'},-,X_{1'}) \quad (60)$$

$$C_{p\text{strong}} = 0.0976X_{\text{strong}}^2 - 37.512X_{\text{strong}} + 3825.4\,\% \; LiBr\text{solutionconcentration} \quad (61)$$

$$C_{p\text{weak}} = 0.0976X_{\text{weak}}^2 - 37.512X_{\text{weak}} + 3825.4\,\% \; LiBr\text{solution concentration} \quad (62)$$

$$t_{3'} = t_A + 0.947906m_{6'}C_{p\text{strong}}(t_G - t_A) / (m_{1'}C_{p\text{weak}}) \quad (63)$$

$$h_{1'} = h_{2'} = h_A \quad (64)$$

Table 2. Coefficient of Equation

constant coefficients	value
A_0	3.462023
A_1	-2.679895×10^{-2}
B_0	1.3449×10^{-3}
B_1	-6.55×10^{-6}
D_0	162.81
D_1	−6.0418
D_2	4.5348×10^{-3}
D_3	1.2053×10^{-3}

Table 3. Energy Relationship of Components in Case 4

component	energy	
HE1	$m_{CO_2}(t)(h_e - h_l) = m_{salt}(t)(h_c - h_d)$	(79)
HE2	$m_{steam}(t)(h_s - h_t) = m_{oil}(t)(h_{33} - h_{32})$	(80)
CT	$W_{CT} = m_{CO_2}(t)(h_e - h_f)\eta_G$	(81)
SCT	$W_{SCT} = m_{steam}(t)(h_m - h_n)\eta_G$	(82)
CC	$W_{CC} = m_{CO_2}(t)(h_k - h_j)/\eta_G$	(83)
pump	$W_{pump} = m_{steam}(t)(h_p - h_o)/\eta_G$	(84)
precooler	$Q_{Pre-cooler} = m_{CO_2}(t)(h_i - h_j)$	(85)
condenser	$Q_{Condenser} = m_{steam}(t)(h_n - h_o)$	(86)
regenerator	$m_{CO_2}(t)(h_g - h_h) = m_{CO_2}(t)(h_l - h_s)$	(87)
WHX	$Q_{WHX} = m_{WHX}(t)(h_{12'} - h_{11'})$	(88)
hot tank (salt)	$C_{hts}(t) = C_{hts}(t-1) + m_{rec}(t) - m_{HE1,s}(t)$	(89)
cold tank (salt)	$C_{cts}(t) = C_{cts}(t-1) - m_{rec}(t) + m_{HE1,s}(t)$	(90)
hot tank (oil)	Chto(t) = Chto(t−1) − mHeater1(t) − mHeater2(t) − mHeater3(t) − mHeater4(t) − mHeater5(t) − mHeater6(t) − mGenerator(t) + mHE2,oil(t) + mCooler1 + mCooler2 + mCooler3	(91)
cold tank (oil)	Ccto(t) = = Ccto(t−1) + mHeater1(t) + mHeater2(t) + mHeater3(t) + mHeater4(t) + mHeater5(t) + mWaterCooler(t) + mWHX(t) − mHE2,oil(t) − mCooler1 − mCooler2 − mCooler3	(92)
ACC	$C_{ACC}(t) = C_{ACC}(t-1)) + m_{Cooler3,air}(t) - m_{Heater,oil}(t)$	(93)

$$h_{3'} = (A_0,+,A_1,X_{\text{weak}})t_{3'} + 0.5(B_0,+,B_1,X_{\text{weak}})t_{3'}^2 + (D_0,+,D_1,X_{\text{weak}},+,D_2,X_{\text{weak}}^2,+,D_3,X_{\text{weak}}^3) \quad (65)$$

$$h_{4'} = h_G \quad (66)$$

$$h_{5'} = h_{6'} = (A_0,+,A_1,X_{\text{strong}})t_{5'} + 0.5(B_0,+,B_1,X_{\text{strong}})t_{5'}^2 + (D_0,+,D_1,X_{\text{strong}},+,D_2,X_{\text{strong}}^2,+,D_3,X_{\text{strong}}^3) \quad (67)$$

$$h_{8'} = h_{9'} \quad (68)$$

$$Q_G(t) = m_{\text{oil,buffer}}^{\text{in}}(t)(h_{\text{oil},h},-,h_{\text{oil},AR}) \quad (69)$$

$$m_r(t) = \frac{Q_G(t)}{h_{7'} + \frac{X_{1'}}{X_{6'} - X_{1'}}h_4 - \frac{X_{6'}}{X_{6'} - X_{1'}}h_{3'}} \quad (70)$$

$$Q_{epro}(t) = m_r(t)(h_{10'},-,h_{9'}) \quad (71)$$

$$m_{6'}(t) = m_r(t)m_{6'} \quad (72)$$

$$m_{1'}(t) = m_r(t)m_{1'} \quad (73)$$

https://doi.org/10.1021/acsomega.3c03401
ACS Omega 2023, 8, 42126−42143

Table 4. Unit Equipment Correlation Coefficient

device	$R_{COP,EB}$	$R_{COP,EC}$	η_{AC}	η_{AT}	$\eta_{Heater}/\eta_{Cooler}$	η_{COM}	η_{CT}	η_{ST}	η_{pump}
value	3.5	3	0.83	0.9	0.9/0.9	0.89	0.93	0.90	0.89

Table 5. Design Parameters of the Proposed CCHP System

parameter	value
environmental pressure	0.1013 MPa
ambient temperature	293.15 K
air gas constant	0.287 kJ/kg·K
specific heat of air at constant pressure	1 kJ/kg·K
specific heat of constant volume air	0.718 kJ/kg·K
specific heat capacity of water	4.2 kJ/kg·K
specific heat capacity of heat transfer oil	2.1 kJ/kg·K
valve outlet pressure	4 MPa

$$\rho = 1145.36 + 470.84(X_{weak} / 100)^2 - (0.333393 + 0.571749(X_{weak} / 100))T_A \quad (74)$$

$$W_{pump}(t) = m_{1'}(t)(P_G, -, P_A) / \rho \quad (75)$$

$$Q_A(t) = m_r(t)h_{10'} + m_{6'}(t)h_{6'} - m_{cir}(t) \quad (76)$$

$$Q_C(t) = m_r(t)(h_{7'}, -, h_{8'}) \quad (77)$$

$$COP_{absorption} = Qepro(t) / (Q_G, (t), +, W_{pump}, (t)) \quad (78)$$

In formula (57), the coefficient is shown in Table 2 and Table 3.

APPENDIX B

Energy Relationship of Components in Case 4

APPENDIX C

System-Related Parameters

AUTHOR INFORMATION

Corresponding Author

Xinglin Yang − *School of Energy and Power, Jiangsu University of Science and Technology, Zhenjiang 212003, China*; Email: yangxl23320@163.com

Authors

Shouqing Zheng − *School of Energy and Power, Jiangsu University of Science and Technology, Zhenjiang 212003, China*

Jiaqi Chang − *School of Energy and Power, Jiangsu University of Science and Technology, Zhenjiang 212003, China*

Complete contact information is available at: https://pubs.acs.org/10.1021/acsomega.3c03401

Notes

The authors declare no competing financial interest.

ACKNOWLEDGMENTS

The authors would like to acknowledge the Postgraduate Research & Practice Innovation Program of Jiangsu Province (Grant No. KYCX21_3504, Grant No. KYCX 20_3100).

NOMENCLATURE

A	area (m^2)
D	diameter (m)
H	height (m)
DNI	direct normal irradiance ($W·m^{-2}$)
Q	heat flow rate (W)
C	Capacity (kg)
t	hour (1−24)
T	temperature (°C)
P	pressure (kPa)
m	mass flow rate ($kg·s^{-1}$)
h	enthalpy ($kJ·kg^{-1}$)
COP	coefficient of performance

GREEK SYMBOLS

η	efficiency(%)
λ	thermal conductivity($W·m^{-1}$ K^{-1})
τ	price($)

SUPERSCRIPTS AND SUBSCRIPTS

1, 2,	state points
a, b, c,	state points
1′, 2′, 3′	state points
rec	receive
am	ambient
EVA	evaporator
AR	Absorption refrigerator
in/out	input/output
w	tube wall
SPT	solar power tower
IES	integrated energy system
G	generator
min	minimum
max	maximum
low	lower limit of climb rate
up	upper limit of climb rate
HE	heat exchanger
WC	water cooler
CT	CO_2 turbine
COM	compressor
ST	steam turbine
AC	air compressor
AT	air turbine
PreH	pre-heater
PreC	precooler
HT	heater
CL	cooler
WHR	waste heat recovery
REG	regenerator
c/h	cold/hot
EV	expansion valve
GEN	generator
AB	absorber
CON	condenser
EB	electricity boiler
EC	electricity chiller

https://doi.org/10.1021/acsomega.3c03401
ACS Omega 2023, 8, 42126−42143

REFERENCES

(1) Brauwer, P.; Ellis, G.; Chateau, Z.; Wade, R.; Luga, C. D. *REN21 Global Status Report 2020, Feature Chapter 8: Public Support for Renewables*; 2020.

(2) Chen, H.; Cong, T. N.; Wei, Y.; Tan, C.; Ding, Y. Progress in electrical energy storage systems: a critical review. *Prog. Nat. Sci.* **2009**, *19* (3), 291−312.

(3) Khan, Muhammad Imran; Asfand, Faisal; Al-Ghamdi, Sami G. Progress in research and technological advancements of thermal energy storage systems for concentrated solar power. *J. Energy Storage* **2022**, *55*, No. 105860.

(4) Yang, J.; Li, J.; Yang, Z.; Duan, Y. Thermodynamic analysis and optimization of a solar organic Rankine cycle operating with stable output. *Energy Convers. Manage.* **2019**, *187*, 459−471.

(5) Merchán, R. P.; Santos, M. J.; Medina, A.; Hernández, A. C. High temperature central tower plants for concentrated solar power: 2021 overview. *Renewable Sustainable Energy Rev.* **2021**, *155*, No. 111828, DOI: 10.1016/j.rser.2021.111828.

(6) Wang, K.; He, Y. L. Thermodynamic analysis and optimization of a molten salt solar power tower integrated with a recompression supercritical CO2 Brayton cycle based on integrated modeling. *Energy Convers. Manage.* **2017**, *135*, 336−350.

(7) Wang, K.; Li, M.-J.; Guo, J.-Q.; Li, P.; Liu, Z.-B. A systematic comparison of different S-CO2 Brayton cycle layouts based on multi-objective optimization for applications in solar power tower plants. *Appl. Energy* **2018**, *212*, 109 DOI: 10.1016/j.apenergy.2017.12.031.

(8) Li, P.; Lin, H.; Li, J.; et al. Analysis of a direct vapor generation system using cascade steam-organic Rankine cycle and two-tank oil storage. *Energy* **2022**, *257*, No. 124776, DOI: 10.1016/j.energy.2022.124776.

(9) Liu, Y.; Wang, Y.; Zhang, Y.; Hu, S. Design and performance analysis of compressed CO2 energy storage of a solar power tower generation system based on the S-CO2 Brayton cycle. *Energy Convers. Manage.* **2021**, *249*, No. 114856.

(10) Luo, X.; Wang, J.; Krupke, C.; Wang, Y.; Sheng, Y.; Li, J.; Xu, Y.; Wang, D.; Miao, S.; Chen, H. Modelling study, efficiency analysis and optimization of large-scale Adiabatic Compressed Air Energy Storage systems with low-temperature thermal storage. *Appl. Energy* **2016**, *162*, 589−600.

(11) Mei, S.; Li, R.; Chen, L.; Xue, X. An overview and outlook on advanced adiabatic compressed air energy storage technique. *Proc. CSEE* **2018**, *38* (10), 2893−2907.

(12) Yu, Q.; Tian, L.; Li, X.; Tan, X. Compressed air energy storage capacity configuration and economic evaluation considering the uncertainty of wind energy. *Energies* **2022**, *15* (13), 4637.

(13) Li, Y.; Miao, S.; Zhang, S.; Yin, B.; Xing, L.; Mark, D.; Wang, J. A reserve capacity model of AA-CAES for power system optimal joint energy and reserve scheduling. *Int. J. Electr. Power Energy Syst.* **2019**, *104*, 279−290.

(14) Wang, X.; Yang, C.; Huang, M.; Ma, X. Multi-objective optimization of a gas turbine-based CCHP combined with solar and compressed air energy storage system. *Energy Convers. Manage.* **2018**, *164*, 93 DOI: 10.1016/j.enconman.2018.02.081.

(15) Jiang, R.; Cai, Z.; Peng, K.; Yang, M. Thermo-economic analysis and multi-objective optimization of polygeneration system based on advanced adiabatic compressed air energy storage system. *Energy Convers. Manage.* **2021**, *229*, No. 113724.

(16) Wu, Y.; Zhang, T. Risk Assessment of Offshore Wave-Wind-Solar-Compressed Air Energy Storage Power Plant through Fuzzy Comprehensive Evaluation Model. *Energy* **2021**, *223* (5), No. 120057.

(17) Gang, P.; Yang, H.; Jing, L.; Rodríguez-Sanchez, M. Performance investigation of the solar power system using cascade supercritical carbon dioxide Brayton-steam Rankine cycle. *Energy Convers. Manage.* **2020**, *225* (2020), No. 113430.

(18) Liu, H.; Wang, M.; Li, S. Investigation of the polygeneration system integrated with gas engine-driven heat pump system and CO2 Brayton cycle for waste heat recovery. *Appl. Therm. Eng.* **2023**, *221*, No. 119872.

(19) Zhang, Z.; Chen, Y.; Ma, J.; Zhao, D.; Qian, M.; Li, D.; Wang, D.; Zhao, L.; Zhou, M. Stochastic optimal dispatch of combined heat and power integrated AA-CAES power station considering thermal inertia of DHN. *Int. J. Electr. Power Energy Syst.* **2022**, *141*, No. 108151.

(20) Liu, Z.; Yang, X.; Liu, X.; Wang, W.; Yang, X. Evaluation of a trigeneration system based on adiabatic compressed air energy storage and absorption heat pump: Thermodynamic analysis. *Appl. Energy* **2021**, *300*, No. 117356.

(21) Lin, X.; Zuo, L.; Yin, L.; Su, W.; Ou, S. An idea to efficiently recover the waste heat of Data Centers by constructing an integrated system with carbon dioxide heat pump, mechanical subcooling cycle and lithium bromide-water absorption refrigeration cycle. *Energy Convers. Manage.* **2022**, *256*, No. 115398.

(22) Yang, J.; Yang, Z.; Duan, Y. Off-design performance of a supercritical CO_2 Brayton cycle integrated with a solar power tower system. *Energy* **2020**, *201*, No. 117676, DOI: 10.1016/j.energy.2020.117676.

(23) Spayde, E.; Mago, P. J.; Cho, H. Performance Evaluation of a Solar-Powered Regenerative Organic Rankine Cycle in Different Climate Conditions. *Energies* **2017**, *10* (1), 94 DOI: 10.3390/en10010094.

(24) Yao, E.; Wang, H.; Liu, L.; Xi, G. A Novel Constant-Pressure Pumped Hydro Combined with Compressed Air Energy Storage System. *Energies* **2014**, *8* (1), 154−171.

(25) Wang, J.; Ren, C.; Gao, Y.; Chen, H.; Dong, J. Performance investigation of a new geothermal combined cooling, heating and power system. *Energy Convers. Manage.* **2020**, *208*, No. 112591, DOI: 10.1016/j.enconman.2020.112591.

(26) Wang, J.; Ren, Y.; Guo, Z.; Zhang, Y. Optimal scheduling of comprehensive energy systems based on comprehensive demand response and reward and punishment tiered carbon trading. *Energy Storage Sci. Technol.* **2022**, *11* (07), 2177−2187.

(27) Wang, J.; Yan, Z.; Pan, Z.; Dai, Y. Off-design performance analysis of a solar-powered organic Rankine cycle. *Energy Convers. Manage.* **2014**, *80*, 150−157.

(28) Garg, P.; Kumar, P.; Srinivasan, K. Supercritical carbon dioxide Brayton cycle for concentrated solar power. *J. Supercrit. Fluids* **2013**, *76*, 54−60.

(29) Zhang, Y.; Zhao, H.; Li, B.; Wang, X. Research on dynamic pricing and operation optimization strategy of integrated energy system based on Stackelberg game. *Int. J. Electr.* **2022**, *143*, No. 108446.

(30) Tian, Y.; Dong, Z.; Yu, Z.; Lyu, M.; Lai, Y.; Zhang, T.; Xue, X.; Xie, N.; et al. Conventional and advanced exergy analysis of large-scale adiabatic compressed air energy storage system. *J. Energy Storage* **2023**, *57*, No. 106165.

(31) Houssainy, S.; Janbozorgi, M.; Ip, P.; Kavehpour, P. Thermodynamic Analysis of a High Temperature Hybrid Compressed Air Energy Storage (HTH-CAES) System. *Renewable Energy* **2017**, *115*, 1043.

(32) Ke, Y.; Zhang, Y.; Li, X.; et al. Theoretical evaluation on the impact of heat exchanger in Advanced Adiabatic Compressed Air Energy Storage system. *Energy Convers. Manage.* **2014**, *86*, 1031−1044.

(33) Zhang, Y.; Zhao, H.; Li, B.; Xu, J. Research on dynamic pricing and operation optimization strategy of integrated energy system based on Stackelberg game. *Int. J. Electr. Power Energy Syst.* **2022**, *143*, No. 108446.

(34) Chen, W. D.; Chua, K. J. A novel and optimized operation strategy map for CCHP systems considering optimal thermal energy utilization. *Energy* **2022**, *259*, No. 124961, DOI: 10.1016/j.energy.2022.124961.

(35) Shi, L.; Shu, G.; Hua, T.; Shuai, D. A review of modified Organic Rankine cycles (ORCs) for internal combustion engine waste heat recovery (ICE-WHR). *Renewable Sustainable Energy Rev.* **2018**, *92*, 95−110.

(36) Wu, J.; Zheng, J.; Mei, F.; Li, K.; Qi, X. Reliability evaluation method of distribution network considering the integration impact of distributed integrated energy system. *Energy Rep.* **2022**, *8*, 422−432.

https://doi.org/10.1021/acsomega.3c03401
ACS Omega 2023, 8, 42126−42143

(37) Liu, R.; Jia, Y.; Fu, K.; Han, X. Double layer optimization of wind storage capacity in transmission networks considering risk reserve constraints. *Grid Technol.* **2021**, *45* (7), 11.
(38) Fan, W.; Ju, L.; Tan, Z.; Li, X.; Zhang, A.; Li, X.; Wang, Y. Two-stage distributionally robust optimization model of integrated energy system group considering energy sharing and carbon transfer. *Appl. Energy* **2023**, *331*, No. 120426.
(39) Zeng, L.; Xu, J.; Wu, M.; Tang, J.; Wu, Q.; Wang, Q.; Fan, G. Day-ahead interval optimization for CCHP system considering uncertainty of wind power and PV. *Int. J. Electr. Power Energy Syst.* **2022**, *138*, No. 107895.

https://doi.org/10.1021/acsomega.3c03401
ACS Omega 2023, 8, 42126−42143